Talanta 117 (2013) 359–365

Contents lists available at ScienceDirect

Talanta

journal homepage: www.elsevier.com/locate/talanta

Simultaneous determination of dopamine and uric acid using layer-by-layer graphene and chitosan assembled multilayer films

Xuexiang Weng [a,*], Qingxue Cao [a], Lixin Liang [a], Jianrong Chen [a], Chunping You [b,**], Yongmin Ruan [a], Hongjun Lin [c], Lanju Wu [a]

[a] College of Chemistry and Life Science, Zhejiang Normal University, Jinhua 321004, PR China
[b] State Key Laboratory of Dairy Biotechnology, Technology Center, Bright Dairy and Food Co. Ltd., Shanghai 200436, PR China
[c] College of Geography and Environmental Sciences, Zhejiang Normal University, Jinhua, 321004, PR China

ARTICLE INFO

Article history:
Received 22 May 2013
Received in revised form
12 September 2013
Accepted 19 September 2013
Available online 25 September 2013

Keywords:
Layer-by-layer
Graphene
Chitosan
Dopamine
Uric acid

ABSTRACT

Multilayer films containing graphene (Gr) and chitosan (CS) were prepared on glassy carbon electrodes with layer-by-layer (LBL) assembly technique. After being characterized with cyclic voltammetry (CV), electrochemical impedance spectroscopy (EIS) and scanning electron microscopy (SEM), the electrochemical sensor based on the resulted films was developed to simultaneously determine dopamine (DA) and uric acid (UA). The LBL assembled electrode showed excellent electrocatalytic activity towards the oxidation of DA and UA. In addition, the self-assembly electrode possessed an excellent sensing performance for detection of DA and UA with a linear range from 0.1 μM to 140 μM and from 1.0 μM to 125 μM with the detection limit as low as 0.05 μM and 0.1 μM based on $S/N=3$, respectively.

1. Introduction

Dopamine (DA) and uric acid (UA) are compounds of great biological and chemical interest and play important roles in physiological function of organisms. DA is a monoamine neurotransmitter found in brain. The basal DA concentration in the extracellular fluid of the central nervous system is about 0.1 μM [1]. The nomal levels of DA are essential for the functions of the central nervous system. UA is the final oxidation product of urine metabolism and is excreted in urine. The normal UA level in serum range from 240 to 520 μM and in urinary excretion is typically 1.4–4.4 mM [2]. Determination of related catecholamine compounds is significant not only in biomedical chemistry and neurochemistry but also for diagnostic and pathological investigations [3,4]. Considerable efforts [5] have been made to develop reliable determination methods for DA and UA. Electrochemical oxidation is one of the most significant and successful detection methods, since the electrodes can be made conveniently to sense them in vivo. However, UA is coexisted with DA in the extracellular fluids of the central nervous system in mammals and can be oxidized at a potential close to that of DA. Therefore, simultaneous determination of these two species using bare electrode remains a challenge.

To solve this problem, different sensing materials have been used to increase the sensitivity and selectivity of the bare electrode, such as nanoparticles [6] and carbon nanotubes [7,8]. Graphene (Gr), a honeycomb lattice of carbon only a single atom thick, is currently the most intensively studied carbon material since discovered in 2004 [9]. The fascinating physical properties of Gr, such as a high specific surface area, extraordinary electronic properties and electron transport capabilities, high elastic behavior and impermeability, make it a promising material for electrochemistry. In recent years, several reviews [10–12] covering Gr with particular emphasis on electrochemical applications have appeared.

Considering its biocompatibility, Gr can be functionalized with biopolymer. Chitosan (CS) [13] is a natural biopolymer which displays excellent film-forming ability, high water permeability, good adhesion, and susceptibility to chemical modification due to the presence of reactive amino and hydroxyl functional groups. It is commonly used to disperse nanomaterials and immobilize enzymes for constructing biosensors.

Recently, the cooperation of Gr and CS as an enhanced sensor substrate has been reported, encompassing enzyme sensors and enzymeless sensors. The enzyme sensors exhibited a wider linearity range compared with other nanostructured supports which were mostly used to detect hydrogen peroxide [14–18] and

* Corresponding author. Tel.: +86 579 82282269.
** Corresponding author. Tel.: +86 21 66553513.
E-mail addresses: xuexian@zjnu.cn (X. Weng), youchunping@brightdairy.com (C. You).

0039-9140/$ - see front matter © 2013 Elsevier B.V. All rights reserved.
http://dx.doi.org/10.1016/j.talanta.2013.09.023

glucose [19,20]. The enzymeless sensors were used to detect nitric oxide [21], erythromycin [22], dopamine [23–28], methyl parathion [29] and nucleic acids [30–32]. The sensing films as reported above were directly cast on the sensing base. In order to promote the widespread application of these two materials, the film formation technique needs to be thoroughly developed.

Layer-by-layer (LBL) adsorption technique offers an easy and inexpensive process to form thickness controllable ultrathin films of a variety of organic and inorganic compounds with targeted properties. The procedure is based on the alternative deposition of the oppositely charged polyelectrolyte, proteins, or charged nanomaterials on a charged surface by attractive electrostatic force [33]. The multilayer film has good thermal and mechanical stability with the characteristics of nanomaterials well maintained. In this work, we prepared stably assembled Gr/CS multilayer films using LBL method based on electrostatic interaction between negatively charged Gr and positively charged CS to study electrochemical catalytic activity for DA and UA. The remarkable sensitivity and selectivity of the assembled electrode were realized for simultaneously determine DA and UA.

2. Experimental

2.1. Reagents

Gr was purchased from Nanjing XFNANO Materials Tech Co., Ltd. CS, DA and UA were bought from Sigma. CS hydrogel was prepared by dissolving 50 mg CS in 10 mL of 1% (V/V) acetic acid solution with sonication for 1 h to obtain positively charged homogeneous hydrogel. Phosphate buffer solution (PBS) was prepared using stock solutions of 0.1 M Na_2HPO_4 and 0.1 M NaH_2PO_4. All other chemicals were of analytical grade and prepared with bidistilled water.

2.2. Instruments

All electrochemical measurements were performed on a CHI 660C Electrochemical Workstation (Chenhua Instrument Co. Shanghai, China). The electrochemical experiments were performed in a three-electrode system consisting of a platinum wire counter electrode, a saturated calomel reference electrode (SCE), and the modified glass carbon working electrode (GCE, diameter 3.0 mm).

The surface morphology of the LBL films was characterized by scanning electron microscopy (SEM, Hitachi S-4800, Japan). A silicon wafer was used for SEM characterization to mimic a GCE surface. The surface was first cleaned in a piranha solution (a 1:3 mixture of 30% H_2O_2 and concentrated H_2SO_4) and then thoroughly rinsed with distilled water. The pre-treated silicon wafer was alternatively incubated in the solutions of Gr and CS for 30 min each, rinsed with water, and then dried in a stream of nitrogen. FTIR spectrum was measured by a Thermo NEXUS 670 Fourier transform infrared spectrometer in the range of 400–4000 cm^{-1}. Raman spectrum was collected on a Renishaw RM1000 confocal microscope with exciting wavelength of 514.5 nm under ambient conditions.

2.3. Construction of the assembled multilayer films

GCE was used to grow the multilayer films. Prior to modification, the GCE was polished with 1, 0.3 and 0.05 μm alumina powders sequentially and then washed with ultrasonication in water and ethanol for 3 min, respectively. Gr (1 mg) was dispersed in DMF by ultrasonication, resulting in a 1 mg/mL suspension. The multilayer films were prepared by LBL assembly technique: the polished electrode was alternatively incubated in negatively charged solution of Gr and positively charged CS for 30 min each. After the cycle was repeated five times, the $(Gr/CS)_5$/GCE was obtained.

3. Results and discussion

3.1. Film characterization

Raman spectrum (Fig. 1A) shows typical features of carbon materials. The G band at 1585 cm^{-1} is assigned to the E_{2g} phonon mode of sp^2 hybridized carbon atoms. The D band appears at 1350 cm^{-1}, due to local defects and disorder particularly at the edge of Gr. FTIR spectrum was acquired to determine the surface state of Gr. Fig. 1B exhibits the characteristic absorption of O–H

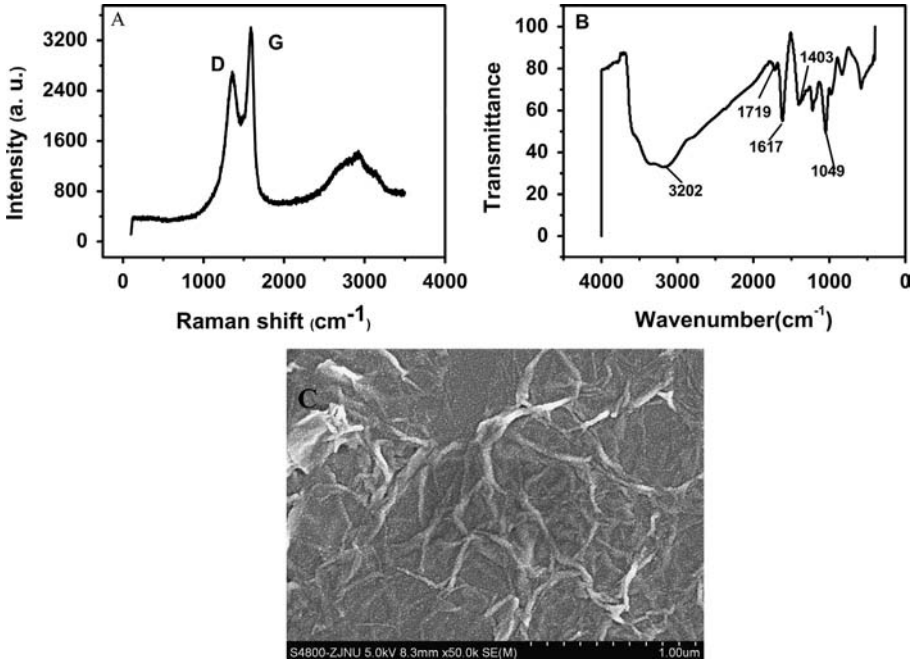

Fig. 1. (A) Raman spectrum and (B) FTIR spectrum of Gr. (C) SEM image of $(Gr/CS)_5$ confined on a silicon wafer to mimic a GCE surface.

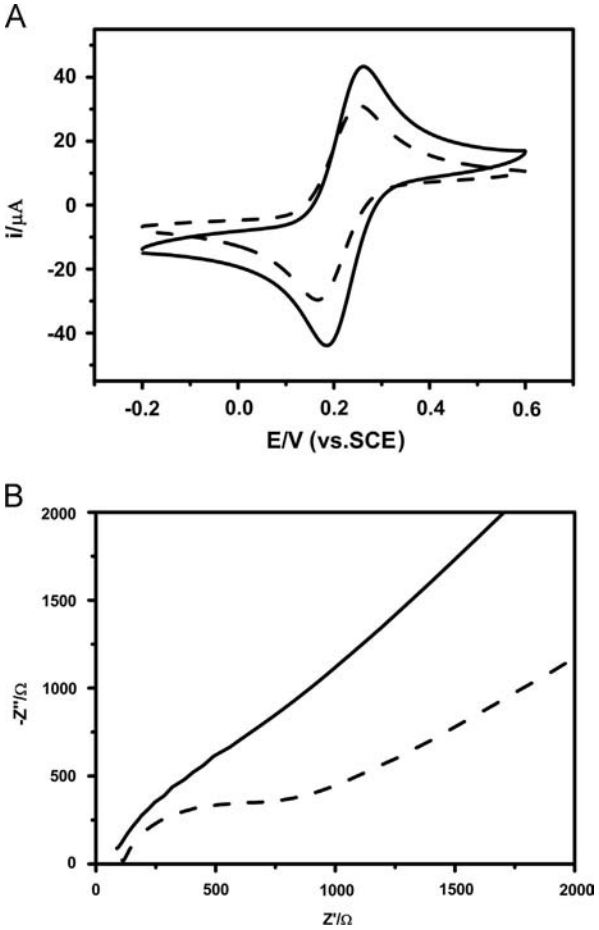

Fig. 2. (A) CVs and (B) nyquist plots of bare GCE (dash line) and $(Gr/CS)_5$/GCE (solid line) in 5.0 mM $[Fe(CN)_6]^{3-/4-}$ solution containing 0.1 M KCl. The frequency range was from 0.01 to 10^5 Hz with perturbation amplitude of 5 mV. The initial potential is 0.11 V.

(ν (carboxyl)) at 1403 cm^{-1}, O–H (broad coupling ν (O–H)) at about 3200 cm^{-1} originated from carboxylic acid, while the band at ca. 3400 cm^{-1} could be due to the O–H stretching mode of intercalated water. The peaks at 1049 cm^{-1} and 1617 cm^{-1} are assigned to C–O and C=C, respectively. Moreover, there is an evidence of C=O of carbonyl groups (1719 cm^{-1}) from acid moieties localized on the edge of graphene sheets [34]. These carboxylic groups provide Gr negatively charged surface [35].

CS is a kind of natural polysaccharide with one primary amino group in the repeating glucosidic residue that rendered its rare positive charge in aqueous acidic media at pH < 6.5. It can adhere to negatively charged surfaces or adsorb negatively charged materials. Fig. 1C shows the SEM image of the LBL alternative growth films of Gr and CS assembled for 5 layers. It is evident that the surface of the modified electrodes is dense and uniform with lots of ripples. Therefore, the LBL assembly technique endows Gr with both the special surface property and the large surface area that is desirable for electrochemical studies.

3.2. Elecrochemical properties of $(Gr/CS)_5$/GCE

$[Fe(CN)_6]^{3-/4-}$ couple is widely used as an electrochemical probe to investigate the properties of the modified electrodes. Fig. 2A compares the voltammetric responses of 5 mM $[Fe(CN)_6]^{3-/4-}$ in 0.1 M KCl at bare GCE and $(Gr/CS)_5$/GCE. The Cyclic voltammetry (CV) curve of the bare GCE (dash line) shows a pair of well defined quasi-reversible peaks. While on the multilayer films of $(Gr/CS)_5$ assembled GCE surface, the redox peak currents increase (solid line), indicating that the modified electrode has a larger electroactive surface area. The electrochemical active surface areas for GCE and $(Gr/CS)_5$/GCE were determined from CVs of 5 mM $K_4[Fe(CN)_6]$ in 0.1 M KCl solution. According to the Randles-Sevcik Eq. (1)·[36]:

$$i_p = (2.69 \times 10^5) n^{3/2} A c D^{1/2} \upsilon^{1/2} \quad (1)$$

where i_p (A) is the peak current, n is the number of electrons participating in the redox reaction, A (cm^2) is the electrode area,

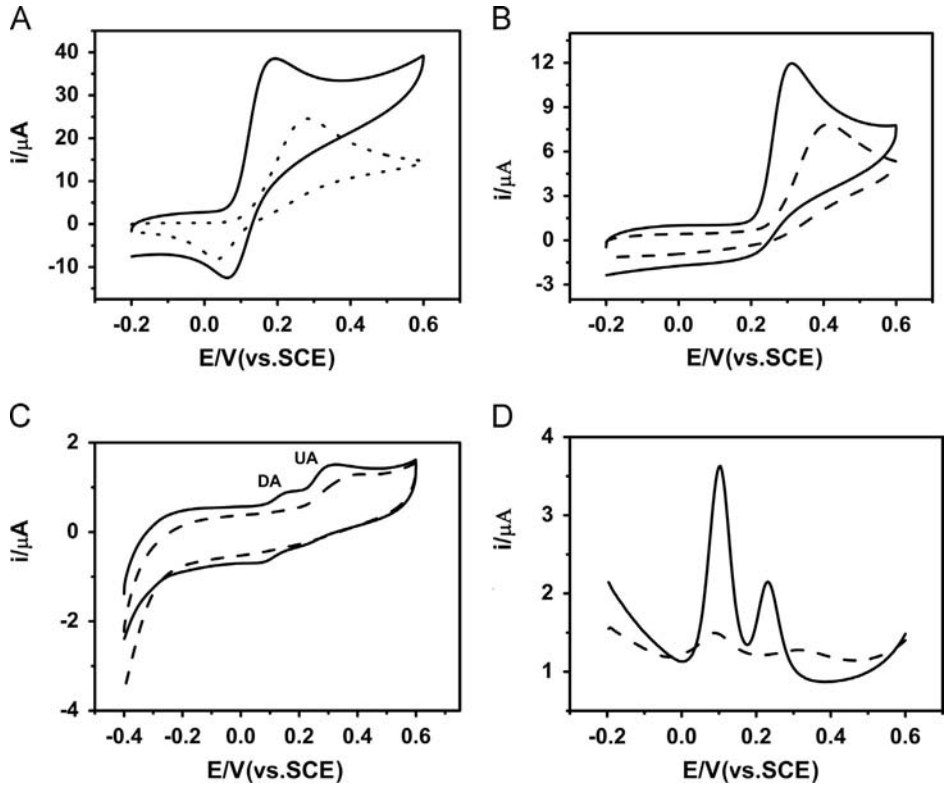

Fig. 3. CVs of (A) 500 μM DA, (B) 400 μM UA and (C) 5 μM DA and 10 μM UA at bare GCE (dash line) and $(Gr/CS)_5$/GCE (solid line) in 0.1 M PBS (pH=7.4) with a scan rate of 100 mV/s. (D) DPVs for 60 μM DA and 60 μM UA in a 0.1 M PBS (pH 7.4) at bare GCE (dash line) and $(Gr/CS)_5$/GCE (solid line), respectively.

D (cm^2/s) is the diffusion coefficient of the oxidized form, hexacyanoferrate (III), c (mol/cm^3) is the bulk concentration of the oxidized form and ν (V/s) is the scan rate. From the slope of the i_p vs. $\nu^{1/2}$ line, the values of A were determined as $(7.8 \pm 0.1) \times 10^{-2}$ cm^2 and $(1.1 \pm 0.3) \times 10^{-1}$ cm^2 for GCE and $(Gr/CS)_5$/GCE, respectively. The increased surface indicates that the assembled multilayer films might be a promising material for electrochemical sensing applications.

Fig. 2B shows the electrochemical impedance spectroscopy (EIS) of bare GCE and the $(Gr/CS)_5$ films modified electrode. A typical EIS curve includes a semicircular part and a linear part. The semicircular part obtained at higher frequency range is the electron-transfer-limited process. Its diameter is equal to the electron-transfer resistance (R_{et}), which controls the electron transfer kinetics of the redox probe on the electrode interface. As shown in Fig. 2B, after assembled with $(Gr/CS)_5$ films (solid line), significant differences were observed. The R_{et} prominently decreases when compared with that of the bare GCE (dash line). The results reveal that $(Gr/CS)_5$ multilayers could form high electron conduction pathways between the electrode and electrolyte, and obviously improve the diffusion of ferricyanide toward the electrode surface.

3.3. Electrochemical oxidation of DA and UA at modified electrodes

Fig. 3A and B compares the CVs of a solution containing 500 μM DA and 400 μM UA in the PBS (pH 7.4) recorded at bare GCE and $(Gr/CS)_5$/GCE. For DA, the cathodic and anodic peaks are located at 0.063 and 0.185 V at $(Gr/CS)_5$/GCE (Fig. 3A, solid line), respectively, showing a smaller peak-to-peak separation than that at bare GCE (dash line, ΔE=250 mV). The anodic peak currents obtained at assembled electrode is 22 μA, which is 1.7 times larger than that at bare GCE. The similar electrocatalytic activity for UA (Fig. 3B) was also found, which occurs with an increased peak current and a small overpotential at $(Gr/CS)_5$/GCE (solid line) compared with bare GCE, indicating the good electron transfer promotion ability of Gr/CS modified materials.

Fig. 3C shows CVs of 5 μM DA and 10 μM UA at bare GCE (dash line) and $(Gr/CS)_5$/GCE (solid line). At the Gr/CS modified electrode the electrochemical signals of the two compounds are well distinguished, and the peak currents are enhanced. This fact shows that it is possible to simultaneously determine DA and UA with the Gr/CS-film-modified electrode. Differential pulse voltammetry (DPV) was further used to investigate the electrocatalytic behavior of DA and UA with a mixture of 60 μM DA and 60 μM UA in PBS (pH=7.4) solution (Fig. 3D). At bare GCE, two weak peaks are observed with poor sensitivity (dash line). While at the $(Gr/CS)_5$/GCE (solid line), the two compounds are oxidized with well-defined and distinguishable sharp peaks at approximately 105 mV and 235 mV for DA and UA, respectively. Both CV and DPV experiments demonstrate that Gr/CS assembled electrode

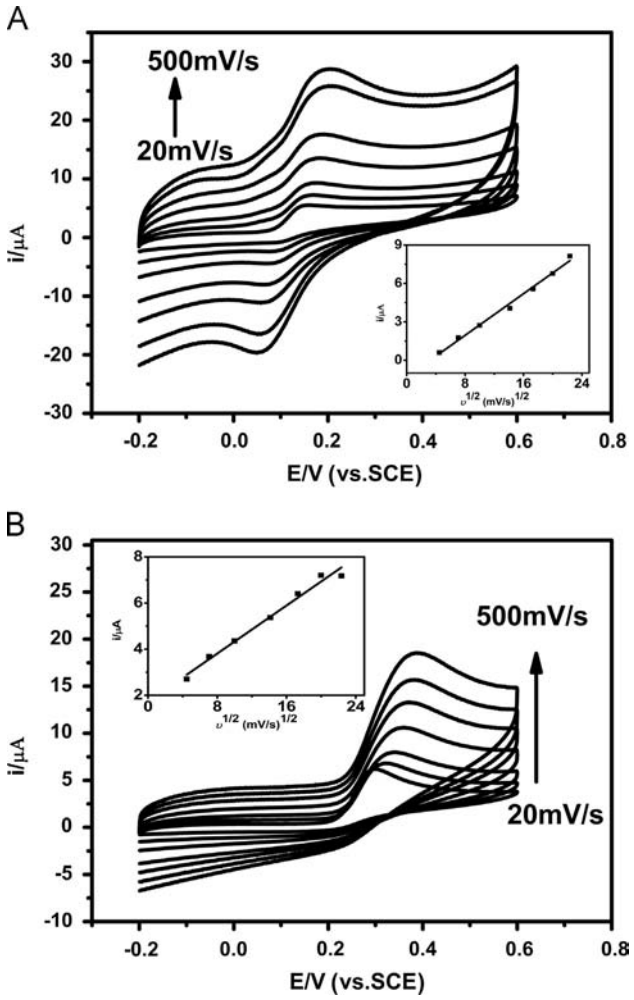

Fig. 4. CVs for the oxidation of (A)150 μM DA and (B) 150 μM UA at the $(Gr/CS)_5$GCE in 0.10 M PBS with different scan rates: 20 mV/s, 50 mV/s, 100 mV/s, 200 mV/s, 300 mV/s, 400 mV/s and 500 mV/s. Inset: Plot of peak current vs. scan rate.

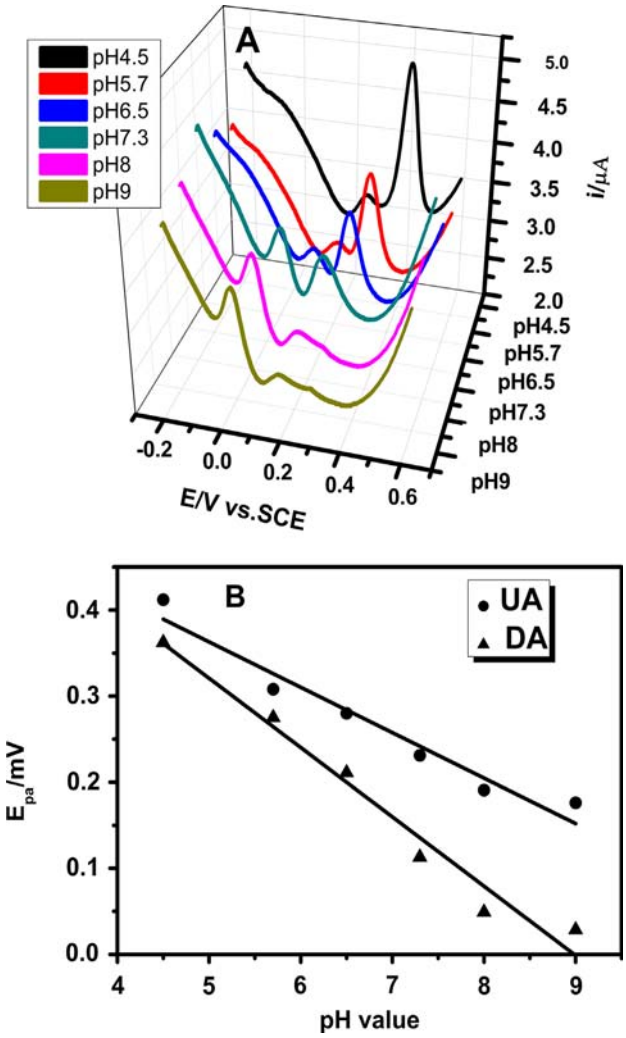

Fig. 5. (A) DPVs of DA (2 μM) and UA (60 μM) at the $(Gr/CS)_5$/GCE in PBS with different pH values (4.5, 5.7, 6.5, 7.3,8.0,9.0) and (B) plots of the oxidation peak potentials for DA and UA as a function of solution pH.

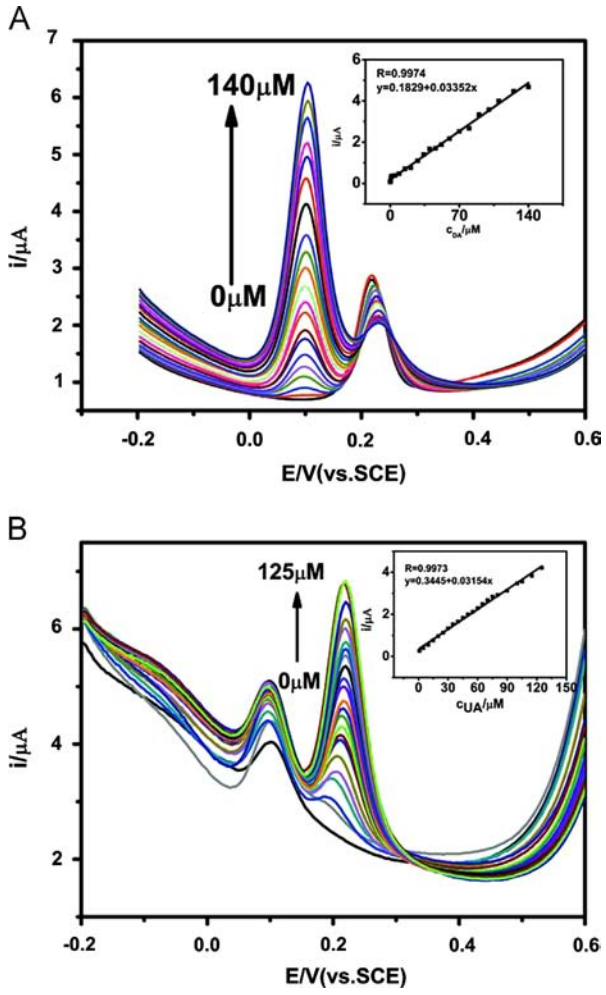

Fig. 6. DPV profiles at $(Gr/CS)_5$/GCE in 0.1 M PBS (pH = 7.4) (A) containing 60 μM UA and different concertrations of DA from 0 μM to 140 μM and (B) containing 50 μM DA and different concertrations of UA from 0 μM to 125 μM.

enhances the electrocatalytic activity towards the oxidation of DA and UA compared to bare GCE.

3.4. Effects of scan rate and pH on the electrochemistry of DA and UA

The effect of scan rate on the CV responses of DA and UA at the $(Gr/CS)_5$GCE was investigated and the results are shown in Fig. 4. The oxidation peak currents of DA and UA increase with the increasing scan rate, while the oxidation peak potentials gradually shift to positive values. Plots of the anodic peak current as a function of the square root of scan rate in the range of 20–500 mV/s show linear relationships, which indicates the electrode reactions of DA and UA are both diffusion-controlled processes.

The influence of pH value on the peak potentials and peak currents of the $(Gr/CS)_5$/GCE sensor for DA and UA was also studied by DPV in the pH range from 4.5 to 9.0 and the results are shown in Fig. 5. As seen in Fig. 5A, with the pH increasing in the measurement solution, all the peak potentials of DA and UA shift to more negative values. This should be a consequence of a deprotonation step involved in all oxidation processes which is facilitated at higher pH values. Fig. 5B shows the effect of pH on the separation of peak potentials with slopes of 52.7 and 58.2 mV/pH, respectively, indicating that the electrochemical oxidation of DA and UA undergoes an equal electron and proton process [37]. Moreover, the peak current of UA decreases when the pH value increases from 4.5 to 9.0. UA and CS possesses a pK_a of approximate 5.7 and 6.5, respectively, thus the repulsive electrostatic interactions on the surface of the CS modified electrode between UA and CS increase with pH. While in the case of DA, the peak current increases when pH > 6.5. The increase at high solution pH could be due to the improved electrostatic attraction between DA and CS, since CS will be deprotonated while DA ($pK_a = 8.8$) will still exist as protonated form at solution pH > 6.5. Based on an overall consideration of physiological pH environment, detection sensitivity and selectivity, pH 7.4 was selected as an optimum pH value for the determination of DA and UA in their mixture.

Table 1
The detection limits and linear ranges of different modified electrodes for simultaneous determination of DA and UA.

Electrode materials	Detection limit (μM)		Linear range (μM)		Ref.
	DA	UA	DA	UA	
$LaPO_4$ nanowires/CPE[a]	0.13	0.9	0.4–11.4	2.7–24.8	[38]
HHNANSA/GCE[b]	0.25	1.17	1.0–130	6.7–20	[39]
MWCNT@PDOP@PtNPS[c]	0.08	0.12	0.25–20	0.3–13	[40]
GCE coated with SDBS[d]	0.05	0.4	0.4–80	4.0–800	[41]
PAPT/ GCE[e]	0.2	0.35	0.95–380	2.0–1000	[42]
P3MT/AuNPs[f]	0.24	0.17	1.0–35	1.0–32	[43]
Au-CA-MWNT[g]	0.02	0.1	0.2–100	1.0–100	[44]
Pyrogallol red modified /CPE[h]	0.78	35	1.0–700	50–1000	[45]
Chitosan-graphene/GCE[i]	1	2	1.0–24	2.0–45	[25]
NG/GCE[j]	0.25	0.045	0.5–170	0.1–20	[26]
$(Gr/CS)_5$/GCE	0.05	0.1	0.1–140	1.0–125	This work

[a] $LaPO_4$ modified carbon paste electrode.
[b] 2-Hydroxy-1-(1-hydroxynapthyl-2-azo)-naphthalin-4-sulfonic acid modified glassy carbon electrode.
[c] Platinum nanoparticles modified multiwalled carbon nanotubes covered with polydopamine.
[d] Nafion/sodium dodecylbenzendsulfonate modified glassy carbon electrode.
[e] Poly(2-amino-5-(4-pyridinyl)-1,3,4-thiadiazole) modified glassy carbon electrode.
[f] Poly(3-methylthiphene)/gold nanoparticles modified glassy carbon electrode.
[g] Cysteamine conjugated with multiwalled carbon nanotubes modified gold electrode.
[h] Pyrogallol red modified carbon paste electrode.
[i] Chitosan–graphene modified glassy carbon electrode.
[j] Nitrogen doped graphene modified glassy carbon electrode.

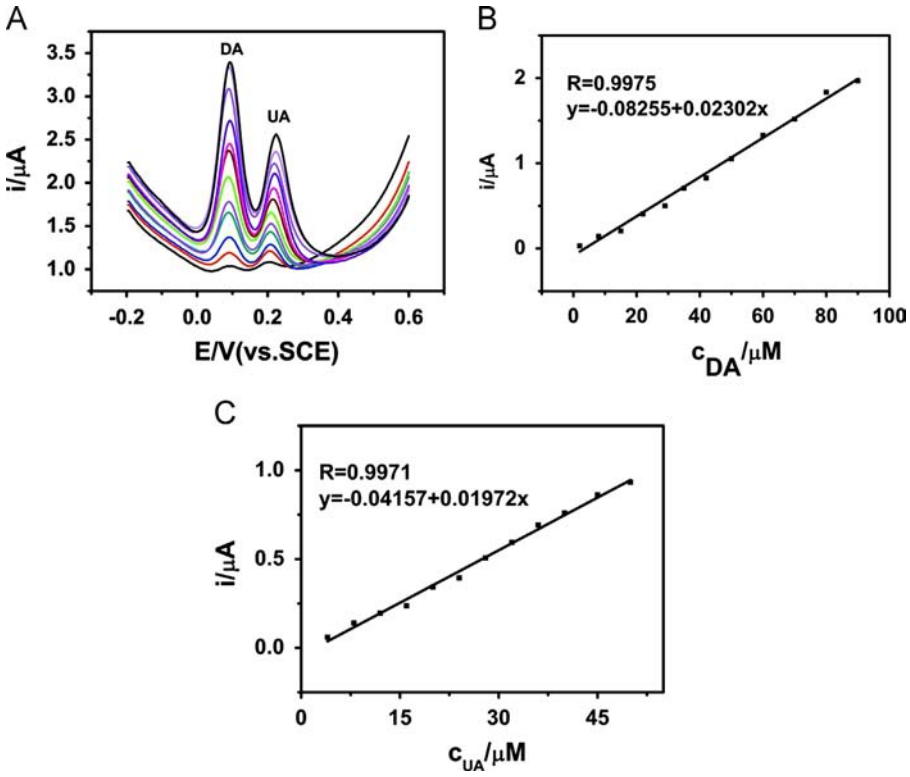

Fig. 7. (A) DPV profiles at $(Gr/CS)_5$/GCE in 0.1 M PBS (pH = 7.4) containing different concentrations of DA and UA. From bottom to up the concentrations from 2.0 to 90 μM for DA and 4.0 to 50 μM for UA, respectively. Plot of the oxidation peak current as a function of (B) DA and (C) UA concentration.

3.5. Individual and simultaneous determination of DA and UA

Since DPV offers a preferable current sensitivity and better separation than CV, it was used for individual and simultaneous determination of DA and UA. The DPV experiments were conducted by first scanning one analyte at a fixed concentration, and then the target analyte was successively added to the electrochemical cell to achieve different concentrations. As shown in Fig. 6, the anodic peak current response of DA or UA increases linearly with the increase of its concentration, while the peak current of the counterpart keeps relatively stable. The small decrease of the counterpart peak current could be due to the dilution effect after successive addition of the target analyte or its consumption from successive DPV oxidation or small changes in pH value solution. The linear ranges for the determination of DA and UA are 1.0×10^{-7}–1.4×10^{-4} M and 1.0×10^{-6}–1.25×10^{-4} M with detection limit of 5.0×10^{-8} M and 1.0×10^{-7} M ($S/N=3$), respectively. The performance of the proposed sensor for detection of DA and UA by DPV was also compared with other electrodes. As shown in Table 1, the analytical parameters (detection limit and linear range) of the $(Gr/CS)_5$/GCE are better or comparable to the results reported for simultaneous determination of DA and UA at the other modified electrode surfaces.

The higher electrocatalytic activity of $(Gr/CS)_5$/GCE is also desirable for simultaneous determination of DA and UA by DPV. As shown in Fig. 7, the amperometric responses of DA and UA still increase linearly with the increase in their concentrations, respectively. The peak currents of DA and UA were linearly proportional to the concentration in the ranges of 2.0–90 μM for DA and 4.0–50 μM for UA with detection limit of 4.0×10^{-7} M and 5.5×10^{-7} M ($S/N=3$), respectively. The excellent properties of such Gr/CS modified electrode can be attributed to two factors: (1) Gr nanosheets with unique structural and electrocatalytic properties play an important role in detecting DA and UA with good sensitivity and selectivity and (2) the LBL alternative growth of Gr and CS gives the multilayer films good thermal and mechanical stability which makes the sensor more reproducible.

3.6. Reproducibility and stability

The fabrication reproducibility for 11 successive measurements were carried out in solutions containing 50 μM DA and 100 μM UA. The results show a relative standard deviation of 5.2% and 4.7% for DA and UA, respectively, indicating that the modified electrode is not subject to surface fouling by the oxidation products, which are notorious for their surface fouling effects at the bare electrode.

4. Conclusions

This study has demonstrated that LBL assembly of Gr/CS sensor not only improved the electrochemical oxidation of DA and UA, but also resolved the overlapping anodic peaks. Therefore, DA and UA contents can be detected individually or simultaneously in their mixture solution. The present work demonstrates that Gr–CS nanofilms fabricated by LBL technique are promising candidates for construction of sensitive and selective electrochemical sensors and other catalytic applications.

Acknowledgments

The authors greatly appreciate the supports of the National Natural Science Foundation of Zhejiang Province (No. LQ12B05002) and National Natural Science Foundation of China (Nos. 21275131, 51108424).

References

[1] A. Ciszewski, G. Milczarek, Anal. Chem. 71 (1999) 1055–1061.
[2] P.T. Kissinger, L.A. Pachla, L.D. Reynolds, S. Wright, J. Assoc. Off Anal. Chem. 70 (1987) 1–14.
[3] R.M. Wightman, L.J. May, A.C. Michael, Anal. Chem. 60 (1988) 769–779.

[4] A. Bossi, S.A. Piletsky, E.V. Piletska, P.G. Righetti, A.P.F. Turner, Anal. Chem. 72 (2000) 4296–4300.
[5] J.F. van Staden, R.I. van Staden, Talanta 102 (2012) 34–43.
[6] M. Stratakis, H. Garcia, Chem. Rev. 112 (2012) 4469–4506.
[7] L. Sanchez, R. Otero, J.M. Gallego, R. Miranda, N. Martin, Chem. Rev. 109 (2009) 2081–2091.
[8] L.B. Hu, D.S. Hecht, G. Grüner, Chem. Rev. 110 (2010) 5790–5844.
[9] K.S. Novoselov, A.K Geim, S.V. Morozov, D. Jiang, Y. Zhang, S.V. Dubonos, I.V. Grigorieva, A.A. Firsov, Science 306 (2004) 666–669.
[10] D. Chen, H.B. Feng, J.H. Li, Chem. Rev. 112 (2012) 6027–6053.
[11] M.S. Artiles, C.S. Rout, T.S. Fisher, Adv. Drug Deliv. Rev. 63 (2011) 1352–1360.
[12] T. Kuila, S. Bose, P. Khanra, A.K. Mishra, N.H. Kim, J.H. Lee, Biosens. Bioelectron. 26 (2011) 4637–4648.
[13] L.L. Wan, Y.H. Song, H.Z. Zhu, Y. Wang, L. Wang, Int. J. Electrochem. Sci. 6 (2011) 4700–4713.
[14] K.F. Zhou, Y.H. Zhu, X.L. Yang, J. Luo, C.Z. Li, S.R. Luan, Electrochim. Acta 55 (2012) 3055–3060.
[15] A.L. Sun, Q.L. Sheng, J.B. Zheng, Appl. Biochem. Biotechnol. 166 (2012) 764–773.
[16] Y.L. Zhou, H.S. Yin, X.M. Meng, Z.N. Xu, Y.R. Fu, S.Y. Ai, Electrochim. Acta 71 (2012) 294–301.
[17] J.H. Yang., N. Myoung, H.G. Hong, Electrochim. Acta 81 (2012) 37–43.
[18] L. Wang., H.Z. Zhu, H.Q. Hou, Z.Y. Zhang, X.P. Xiao, Y.H. Song, J. Solid State Electrochem. 16 (2012) 1693–1700.
[19] X.H. Kang, J. Wang, H. Wu, I.A. Aksay, J. Liu, Y.H. Lin, Biosens. Bioelectron. 25 (2009) 901–905.
[20] Q. Zeng, J.S. Cheng, X.F. Liu, H.T. Bai, J.H. Jiang, Biosens. Bioelectron. 26 (2011) 3456–3463.
[21] W. Wen, W. Chen, Q.Q. Ren, X.Y. Hu, H.Y. Xing, X.H. Zhang, S.F. Wang., Y.D. Zhao, Sens. Actuators B 166-167 (2012) 444–450.
[22] W.J. Lian, S. Liu, J.H. Yu, X.R. Xing, J. Li, M. Cui, J.D. Huang, Biosens. Bioelectron. 38 (2012) 163–169.
[23] B. Liu, H.T. Lian, J.F. Yin, X.Y. Sun, Electrochim. Acta 75 (2012) 108–114.
[24] X.L. Niu, W. Yang, H. Guo, J. Ren, F.S. Yang, J.Z. Gao, Talanta 99 (2012) 984–988.
[25] D.X. Han, T.T. Han, C.S. Shan, A. Ivaska, L. Niu, Electroanalysis 22 (2010) 2001–2008.
[26] Z.H. Sheng, X.Q. Zheng, J.Y. Xu, W.J. Bao, F.B. Wang, X.H. Xia, Biosens. Bioelectron. 34 (2012) 125–131.
[27] M. Pumera, A. Ambrosi, A. Bonanni, E.L.K. Chng, H.L. Poh, TrAC Trends Anal. Chem. 29 (2010) 954–956.
[28] N.G. Shang, P. Papakonstantinou, M. Mcmullan, M. Chu, A. Stamboulis, A Potenza, S.S. Dhesi, H. Marchetto, Adv. Funct. Mater. 18 (2008) 3506–3514.
[29] S.L. Yang, S.L. Luo, C.B. Liu, W.Z. Wei, Colloids Surf. B: Biointerfaces 96 (2012) 75–79.
[30] X.L. Niu, W. Yang, J. Ren, H. Guo, S.J. Long, J.J. Chen, J.Z. Gao., Electrochim. Acta 80 (2012) 346–353.
[31] S. Alwarappan, K. Cissell, S. Dixit, C.Z. Li, S. Mohapatra, J. Electroanal. Chem. 686 (2012) 69–72.
[32] X.W. Qi, H.W. Gao, Y.Y. Zhang, X.Z. Wang, Y. Chen, W. Sun, Bioelectrochemistry 88 (2012) 42–47.
[33] X.Q Zhou, T. Yu, Y.H. Zhang, J.L. Kong, Y. Tang, J.L. Marty, B.H. Liu, Electrochem. Commun. 9 (2007) 1525–1529.
[34] Y.C. Si, E.T. Samulski, Nano. Lett. 8 (2008) 1679–1682.
[35] R. Arrigo, M. Havecker, S. Wrabetz, R. Blume, M. Lerch, J. McGregor, E.P.J. Parrott, J. Axel Zeitler, L.F. Gladden, A. Knop-Gericke, R. Schlogl, D.S. Su, J. Am. Chem. Soc. 132 (2010) 9616–9630.
[36] A.J. Bard, L.R. Faulkner, Electrochemical Methods, Funddamentals and Applications, second ed., John Wiley and Sons, 2001.
[37] C.R. Raj, K. Tokuda, T. Ohsaka, Bioelectrochemistry 53 (2001) 183–191.
[38] Y.Z. Zhou, H.Y. Zhang, H.D. Xie, B Chen, L Zhang, X.H. Zheng, P. Jia, Electrochim. Acta 75 (2012) 360–365.
[39] A.A. Ensafi, S. Dadkhah-Tehrani, B. Rezaei, J. Serb. Chem. Soc. 75 (2010) 1685–1699.
[40] M.H. Lin, H.L. Huang, Y.J. Liu, C.J. Liang, S.D. Fei, X.F. Chen, C.L. Ni, Nanotechnology 24 (2013) 065501.
[41] X.M. Cao, L.Q. Luo, Y.P. Ding, D.W. Yu, Y.B. Gao, Y. Meng, J. Appl. Electrochem. 39 (2009) 1603–1608.
[42] L. Zhang, L.L. Wang, J. Solid State Electrochem. 17 (2013) 691–700.
[43] X. Huang, Y.X. Li, P. Wang, L. Wang, Anal. Sci. 24 (2008) 1563–1568.
[44] S. Shahrokhian, A. Mahdavi-Shakid, M. Ghalkhani, R.S. Saberi, Electroanalysis 24 (2012) 425–432.
[45] A.A. Ensafi, A. Arabzadeh, H. Karimi-Maleh, Electrochemistry 43 (2010) 1976–1988.